Chinese Chemical Letters 33 (2022) 262–265

Contents lists available at ScienceDirect

Chinese Chemical Letters

journal homepage: www.elsevier.com/locate/cclet

Highly active electrocatalytic CO_2 reduction with manganese *N*-heterocyclic carbene pincer by *para* electronic tuning

Can Huang[1], Jiahao Liu[1], Hai-Hua Huang, Xianfang Xu, Zhuofeng Ke*

School of Materials Science & Engineering, School of Chemistry, PCFM Lab, Sun Yat-sen University, Guangzhou 510275, China

ARTICLE INFO

Article history:
Received 28 April 2021
Revised 10 June 2021
Accepted 15 June 2021
Available online 21 June 2021

Keywords:
Pyridine *N*-heterocyclic carbene
Electrocatalysis
Carbon dioxide conversion
Manganese
Substituent effect

ABSTRACT

Electronic tuning by *para* substitutions was explored to achieve a highly active manganese *N*-heterocyclic carbene pincer complex for the selective electrocatalytic reduction of CO_2 to CO. [$MnCNC^{OMe}$]BF_4 (**L2-Mn**) bearing an electron-donating group (–OMe) showed high activity with 63 × catalytic current enhancement, average Faradaic efficiency of 104%, and a TOF_{max} value of 26,127 s^{-1}, which is 127 times higher than that of unsubstituted [$MnCNC^{H}$]Br (**L1-Mn**) reported previously. In contrast, the electron-withdrawing group (–COOMe) in [$MnCNC^{COOMe}$]PF_6 (**L3-Mn**) inhibited the electrocatalytic activity. Ambient Brønstic acid, however, suppressed the activity of **L2-Mn** probably due to the protonation of the –OMe group. These findings indicate a potential electronic tuning strategy to improved manganese *N*-heterocyclic carbene catalysts for CO_2 reduction.

Carbon dioxide reduction is of particular interest in terms of greenhouse alleviation and the production of carbon feedstock. Therefore, the homogeneous and heterogeneous electrocatalytic CO_2 conversion is becoming more and more attractive recently [1–6]. Various electrochemical CO_2 reduction can be involved in different pathways including two, four, six and eight-electron processes, leading to various carbon-based products such as, CO, HCOOH, CH_3OH, HCHO, CH_4, and other value-added chemicals or liquid fuels which could benefit our society sustainability [2,7,8].

Among different families of molecular catalysts for electrocatalytic CO_2 reduction, earth-abundant transition metal complexes, particularly the manganese-based bipyridine complexes, have attracted many interests [9–12]. However, they displayed limited efficiency although extensive exploration has been performed on modifying pyridyl and bipyridyl ligands. *N*-Heterocyclic carbene (NHC) complexes exhibit unique selectivity and stability in catalysis [13–16], owing to the strong σ-donation and the weak π-back-donation properties of the NHC ligands [17]. Recently, manganese complexes supported by NHC ligands have been reported with potential electrocatalytic performances (Fig. 1a) [18–21].

In 2018, Luca *et al.* reported an NHC-based manganese(I) pincer complex [$MnCNC^{H}$]Br (**L1-Mn**) for the selectively electrocatalytic reduction of CO_2 to CO [22]. Inspired by this pincer framework, and guided by our previous theoretical understanding of the *para* electronic effect [23,24], herein, we developed new types of manganese pincer complexes to achieve highly active and selective electro-reduction of CO_2 by tuning the *para* electronic effect (Fig. 1b).

By the introduction of pyridyl *para* substituents on complex **L1-Mn** [22,25], we designed and synthesized new complexes **L2-Mn** and **L3-Mn** (Scheme 1) incorporating an electron-donating methoxy (-OMe) group and an electron-withdrawing methyl formate (-COOMe) group, respectively. Ligands **L1**, **L2** and **L3** were synthesized from dibromopyridine, 2,4,6-trifluoropyridine, and methyl 2,6-dihydroxyisonicotinate, respectively (Schemes S1 and S2 in Supporting information). Complexes **L1-Mn**, **L2-Mn** and **L3-Mn** were obtained with conventional $Mn(CO)_5Br$ as starting materials by overnight reactions in the presence of excess Cs_2CO_3 in MeCN under argon atmosphere (Scheme 1). ^1H NMR, ^{13}C NMR, infrared spectroscopy and single-crystal X-ray diffraction analyses (Scheme 1, Tables S1, S2, Figs. S1-S10 in Supporting information) verified the successful synthesis of this series of complexes. Single-crystal X-ray diffraction analysis confirmed the octahedral structures of **L2-Mn** and **L3-Mn**, with Mn-C_{NHC} bond lengths of

* Corresponding author.
E-mail address: kezhf3@mail.sysu.edu.cn (Z. Ke).
[1] These authors contributed equally to this work.

https://doi.org/10.1016/j.cclet.2021.06.046
1001-8417/

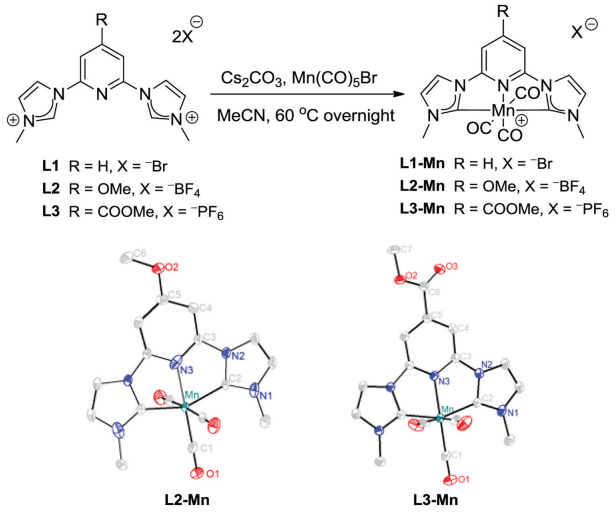

Scheme 1. Synthesis of Mn(I) NHC complexes and X-ray structures of **L2-Mn** and **L3-Mn**.

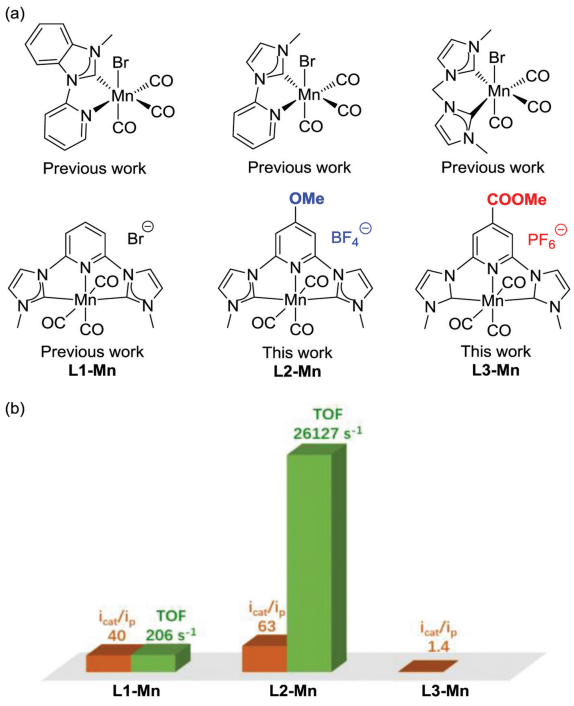

Fig. 1. NHC Mn(I) complexes for electrocatalytic reduction of CO_2.

1.999(5), 2.009(9) Å, and Mn-N bond lengths of 2.001(0), 2.012(4) Å, respectively (Scheme 1). The structures and bond lengths of both complexes are in accordance with the previously reported **L1-Mn** [22] with Mn-C_{NHC} bond length of 1.989(3) Å and Mn-N bond length of 2.017(3) Å.

Cyclic voltammetry analyses of the series of Mn(I) complexes were performed under argon and CO_2 atmosphere, respectively (Fig. 2). Under Ar atmosphere, the cyclic voltammetry of **L1-Mn** showed an irreversible redox wave at $E_{p1} = -2.02$ V (Fig. 2a, all reduction potentials are reported *vs.* Fc^+/Fc), in agreement with previous studies [22]. The redox wave in the CV of complex **L2-Mn** with -OMe shifted cathodically by approximately 200 mV (Fig. 2b, $E_{p2} = -2.16$ V under Ar atmosphere) compared to the redox waves in the CV of complex **L1-Mn**, reflecting the strong electron-donating ability of the -OMe group. The CV of **L3-Mn** with-COOMe shows three pairs of redox waves at −1.64 V, −1.86 V, and −2.14 V, respectively (Fig. 2c and Fig. S23 in Supporting information). Under CO_2 atmosphere, the catalytic current in the CV of **L1-Mn** increased by about 40-fold with the redox wave at $E_{cat1} = -2.37$ V. Surprisingly, the CV of **L2-Mn** shows a dramatic current increase (*ca.* 63-fold) at $E_{cat2} = -2.83$ V, suggesting that the promising promotion of catalytic activity of complex **L2-Mn** for CO_2 reduction caused by the influence of the electron-donating effect. However, the CV of complex **L3-Mn** displayed only minor catalytic current increase (Fig. 1c, *ca.* 1.4-fold), which is in sharp contrast to the behavior of **L1-Mn**, indicating the negative effect of the electron-withdrawing group on the electro-reduction.

Table 1
Results of cyclic voltammetry and controlled potential electrolyses.

Catalyst	E_p (V)	i_{cat}/i_p	E_{cat} (V)	TOF_{max} (s^{-1})	FE (%)[a]
L1-Mn	−2.02[b]	40[b]	−2.37[b]	206[b]	94.2[b]
		56[c]	−2.50[c]	454[c]	94.7[c]
L2-Mn	−2.16[b]	63[b]	−2.83[b]	26,127[b]	104.3[b]
		50[c]	−3.10[c]	408[c]	107.0[c]
L3-Mn	−1.64[b]	1.4[b]	−1.66[b]	–	–
		2.3[c]	−1.69[c]	–	–

[a] FE represents for average Faradaic efficiency resulted from CPE experiments.
[b] Data results from CV of the catalysts in anhydrous 0.1 mol/L $TBAPF_6$/MeCN.
[c] Data results from CV of the catalysts in 0.1 mol/L $TBAPF_6$/MeCN with 240 μL TFE added.

Cyclic voltammetry analyses of complexes **L1-Mn** and **L2-Mn** at scan rates of 8–12 V/s under both CO_2 and Ar atmosphere were performed (Figs. S11, S12, S17 and S18 in Supporting information). An ideally steady-state catalytic progress will lead to an S-shaped CV response, which is independent of the scan rate, with plateau current to determine the maximum turnover frequency (TOF_{max}). CVs of both complexes showed the S-shaped catalytic waves, indicating the ideally and purely kinetic CO_2 catalytic reduction progresses (Figs. S12 and S18). We operated the i_{cat}/i_p analyses to calculate the TOF_{max} for **L1-Mn** and **L2-Mn** from the reported equations [26–29]. **L1-Mn** showed a TOF_{max} of 206 s^{-1} under the CO_2 atmosphere in anhydrous MeCN (Fig. S40 in Supporting information). Notably, the calculated TOF_{max} of **L2-Mn** is 26,127 s^{-1}, which is approximately 127 times higher than the value of **L1-Mn** under the same conditions (Fig. S42 in Supporting information). Reduction potentials, catalytic currents, and calculated TOF_{max} under different conditions are summarized in Table 1.

The addition of Brønstic acid, for example, 2,2,2-trifluoroethanol (TFE) as the proton source, would generally result in the enhancement of catalysis, as reported previously [11,12,22,30,31]. We performed cyclic voltammetry of complexes **L1-Mn** and **L2-Mn** at incremental TFE additions until the catalytic current no longer increased to study the optimum concentration for catalytic conditions (Figs. S13 and S19 in Supporting information). The addition of TFE promoted the catalytic activity of complex **L1-Mn**, as shown in Fig. S13. 240 μL TFE was added to achieve the optimal catalytic conditions. Cyclic voltammetry of **L1-Mn** under Ar and CO_2 atmosphere in 0.1 mol/L $TBAPF_6$/MeCN with 240 μL TFE added gave a 56-fold catalytic current enhancement (Fig. S14 in Supporting information). However, complex **L2-Mn** displayed poor catalytic property when TFE was added as the proton source. The value of i_{cat}/i_p for **L2-Mn** at the presence of TFE decreased to 50 × (Fig. S20 in Supporting information). This phenomenon can be attributed to the protonation of the -OMe group, which thereby suppresses its electron-donation ability. **L1-Mn** and **L2-Mn** with 240 μL TFE added display S-shaped CVs response at scan rates of 8–12 V/s, which represented an ideally steady-state catalysis (Figs. S15 and S21 in Supporting information). With 240 μL TFE added, the calcu-

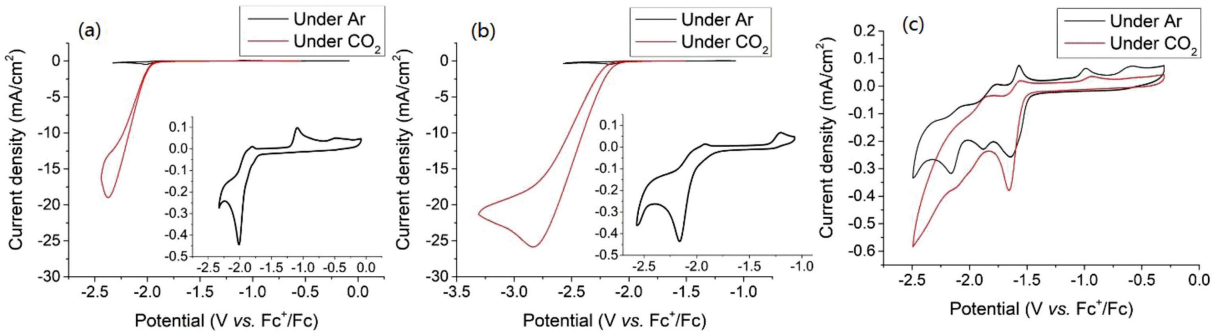

Fig. 2. Cyclic voltammetry of **L1-Mn** (a), **L2-Mn** (b) and **L3-Mn** (c) under Ar (black) and CO_2 (red) atmosphere at 0.1 V/s in dry MeCN with 0.1 mol/L tetrabutylammonium hexafluorophosphate ($TBAPF_6$) supporting electrolyte. All complexes were loaded at a concentration of 1 mmol/L. Glass carbon working electrode, platinum counter electrode, and Ag^+/Ag reference electrode was used.

lated TOF_{max} of **L1-Mn** is enhanced to 454 s^{-1} (Fig. S41 in Supporting information). Owing to the possible protonation of -OMe mentioned above, the calculated TOF_{max} value of **L2-Mn** decreased to 408 s^{-1} with 240 μL TFE addition (Fig. S43 in Supporting information). Cyclic voltammetry of **L3-Mn** with 240 μL TFE added showed a low value of catalytic current enhancement (i_{cat}/i_p = 2.3), indicating its inefficient electrocatalytic properties for CO_2 reduction. Further control experiments with tetrabutylammonium bromide (TBABr) to introduce Br^- anion into the catalytic system of **L2-Mn** were performed (Figs. S25 and S26 in Supporting information), indicating the counter anions did not affect the electrochemical properties [32,33].

Controlled potential electrolysis (CPE) of **L1-Mn**, **L2-Mn,** and **L3-Mn** were performed under CO_2 atmosphere at an applied potential of E_{appl} = −2.37 V under the conditions of anhydrous MeCN and with the addition of TFE as a proton source to study their selectivity and durability (Figs. S27–S36 in Supporting information). Quantification of the gaseous products was conducted by an online gas chromatography thermal conductivity detector (GC-TCD) analysis of the headspace. After an electrolysis over 2 h in anhydrous MeCN, approximately 40.9% current density of the starting state was retained for **L1-Mn** (Fig. S27), which gave an average Faradaic efficiency (FE) of 94.2% (Fig. S28). **L2-Mn** displayed better selectivity and durability with approximately 86.6% current density retained over 2 h (Fig. S31) and an average FE of 104.3% was obtained (Fig. S32). These results demonstrate that the electron-donating effect also enhances the selectivity and durability of the Mn NHC pincer catalyst. With 240 μL TFE added, further promotion of selectivity and durability for **L1-Mn** were shown by the CPE results. 77.2% current density retained over 2 h (Fig. S29) and an average FE of 94.7% was obtained (Fig. S30). Consistent with the results of CVs, **L2-Mn** gave a low level of current density probably because of the protonation of the -OMe. On the other hand, **L3-Mn** showed poor catalytic activity whether TFE was added or not (Figs. S35 and S36). Average Faradaic efficiencies are summarized in Table 1.

According to the studies by Musgrave and Luca *et al.*, a binuclear proton-less reduction pathway is suggested for the $[MnCNC(CO)_3]Br$ pincer system [34]. Therefore, a comparison of the CO_2 reduction cycle for **L1-Mn**, **L2-Mn** and **L3-Mn** based on the bimetallic mechanism using density functional study (DFT) has been conducted to reveal the effects of the *para* substituents (Fig. 3a). First, the Mn(I) species **I** are reduced to species **II** with the required potentials of −2.21 V, −2.25 V and −1.53 V for **L1-Mn** to **L3-Mn**, respectively, which are in agreement with the reduction potentials observed by the CV experiments (Fig. 2). These results reveal the increasing reduction potential of electron-richer species with the *para* electron-donating effect. After the loss of two CO molecules from **II**, which was observed by Luca *et al.* in the case of **L1-Mn**, complexes **III** adopting square planar geometry are generated with the calculated Gibbs free energies to be endergonic by 9.3–13.7 kcal/mol. Then, a complexation process of a CO_2 molecule sandwiched between two **III** intermediates generates complexes **IV**, which are calculated to be 10.4 (9.3 kcal/mol to 19.7 kcal/mol), 5.6 (13.4 kcal/mol to 19.0 kcal/mol), and 30.0 kcal/mol (13.7 kcal/mol to 43.7 kcal/mol) endergonic, re-

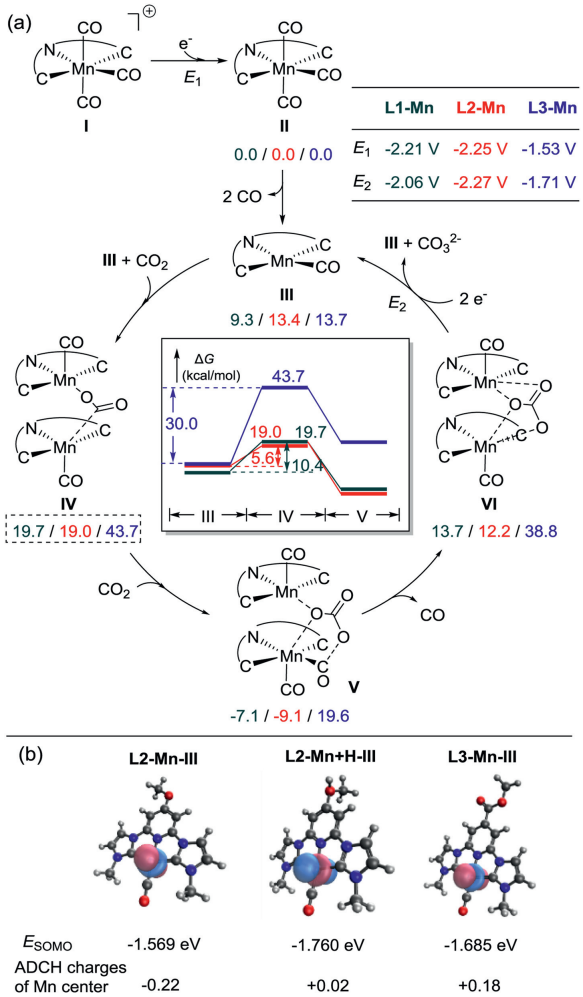

Fig. 3. (a) Comparison of CO_2 reduction cycle for **L1-Mn** (deep green), **L2-Mn** (red), and **L3-Mn** (blue) based on the binuclear proton-less reduction pathway. The Gibbs free energies and the calculated applied electro potentials are kcal/mol and V *vs.* Fc^+/Fc, respectively. (b) SOMOs and ADCH charges of the Mn center of **L2-Mn-III, L2-Mn+*H*-III**, and **L3-Mn-III**.

spectively. Such results indicate the disfavor of the complexation for **L3-Mn** bearing a pyridyl *para* EWG. Subsequently, the insertion of a second CO_2 molecule into species **IV** leading to species **V** with effective disproportionation into a carbonate anion sandwiched between two metal centers and a CO product bounded to one of them. After the release of the CO product, complexes **VI** will be formed. With the calculated potentials of −2.06 V, −2.27 V and −1.71 V for **L1-Mn**, **L2-Mn** and **L3-Mn**, respectively. Two **III** species can be regenerated with the release of the carbonate to furnish the catalytic cycle.

To further reveal the electronic effect of the pyridyl *para* substituents, the molecular orbital analysis and the atomic dipole moment corrected Hirshfeld (ADCH) charges [35,36] analysis of the Mn center were performed for the reduced species **III** of **L1-Mn** (−0.19), **L2-Mn** (−0.22) and **L3-Mn** (+0.18) were analyzed with Multiwfn [36,37], as shown in Fig. 3b. The ADCH charge of the Mn center increases to −0.22 in **L2-Mn-III** from −0.19 in **L1-Mn-III**, indicating the profound impact of the electron-donating *para* pyridyl substituent on improving the nucleophilicity of the Mn center to activate the CO_2 molecule. The low electron density of the Mn center (+0.18) in **L3-Mn-III** and its relatively stable SOMO (−1.685 eV) can account for the low activity of **L3-Mn** for the electrocatalytic reduction of CO_2 due to the EWG. Notably, the protonation of the -OMe (species **L2-Mn+H-III**) significantly increases the ADCH charge of the Mn center to +0.02 from −0.22 in **L2-Mn-III**. And the energy of the SOMO of **L2-Mn+H-III** also decreases to −1.760 eV, which is in good agreement with the experimentally observed suppression of the catalysis due to the negative effect of the TFEs as a proton source.

We also performed Fourier-transform infrared reflectance spectroelectrochemistry (FTIR-SEC) to detect the main species involved in the catalytic reduction process of **L2-Mn** (Figs. S37 and S38 in Supporting information). Under Ar atmosphere, the spectral features at 2117 cm^{-1}, attributing to a CO ligand released [38], corresponding to the report by Myren *et al.* [34]. Under the CO_2 atmosphere, the bands at 1649 cm^{-1} and 1680 cm^{-1} appeared, showing the formation of CO_3^{2-}/HCO_3^- species, which is consistent with the DFT-calculated results.

In summary, a series of manganese *N*-heterocyclic carbene pincer complexes were developed. The *para* electron-donating strategy was achieved in a highly active complex (**L2-Mn**) having -OME group for the selective electrocatalytic reduction of CO_2 to CO, with a larger catalytic current enhancement (63 ×) and a TOF_{max} (26,127 s^{-1}, 127 times of unsubstituted **L1-Mn)**. CPE study of **L2-Mn** gave an average Faradaic efficiency of 104%. While **L3-Mn** with electron-withdrawing -COOMe group inhibited the electrocatalytic activity. Ambient Brønstic acid suppressed the activity of **L2-Mn** probably due to the protonation of the –OMe group. These findings highlight the potential of electronic tuning for the design of efficient manganese NHC catalysts for CO_2 reduction.

Declaration of competing interest

The authors declare that they have no known competing financial interests or personal relationships that could have appeared to influence the work reported in this paper.

Acknowledgments

This work was supported by the National Natural Science Foundation of China (No. 21973113) and the Guangdong Natural Science Funds for Distinguished Young Scholar (No. 2015A030306027), and the Fundamental Research Funds for the Central Universities.

Supplementary materials

Supplementary material associated with this article can be found, in the online version, at doi:10.1016/j.cclet.2021.06.046.

References

[1] C.A. Carpenter, P. Brogdon, L.E. McNamara, et al., Inorganics 6 (2018) 22.
[2] R. Francke, B. Schille, M. Roemelt, Chem. Rev. 118 (2018) 4631–4701.
[3] K. Elouarzaki, V. Kannan, V. Jose, et al., Adv. Energy Mater. 9 (2019) 1900090.
[4] S. Fukuzumi, Y.M. Lee, H.S. Ahn, W. Nam, Chem. Sci. 9 (2018) 6017–6034.
[5] A. Sinopoli, N.T. La Porte, J.F. Martinez, et al., Coord. Chem. Rev. 365 (2018) 60–74.
[6] H. Takeda, C. Cometto, O. Ishitani, M. Robert, ACS Catal. 7 (2016) 70–88.
[7] E.E. Benson, C.P. Kubiak, A.J. Sathrum, J.M. Smieja, Chem. Soc. Rev. 38 (2009) 89–99.
[8] J. Qiao, Y. Liu, F. Hong, J. Zhang, Chem. Soc. Rev. 43 (2014) 631–675.
[9] M. Bourrez, F. Molton, S. Chardon-Noblat, A. Deronzier, Angew. Chem. Int. Ed. 50 (2011) 9903–9906.
[10] J.M. Smieja, M.D. Sampson, K.A. Grice, et al., Inorg. Chem. 52 (2013) 2484–2491.
[11] M.D. Sampson, C.P. Kubiak, J. Am. Chem. Soc. 138 (2016) 1386–1393.
[12] K.T. Ngo, M. McKinnon, B. Mahanti, et al., J. Am. Chem. Soc. 139 (2017) 2604–2618.
[13] D.J. Nelson, S.P. Nolan, Chem. Soc. Rev. 42 (2013) 6723–6753.
[14] M.N. Hopkinson, C. Richter, M. Schedler, F. Glorius, Nature 510 (2014) 485–496.
[15] C. Johnson, M. Albrecht, Coord. Chem. Rev. 352 (2017) 1–14.
[16] E. Peris, Chem. Rev. 118 (2017) 9988–10031.
[17] C. Huang, J. Liu, H.H. Huang, Z. Ke, Polyhedron 203 (2021) 115147.
[18] J. Agarwal, T.W. Shaw, C.J. Stanton, et al., Angew. Chem. Int. Ed. 53 (2014) 5152–5155.
[19] J. Agarwal, C.J. Stanton Iii, T.W. Shaw, et al., Dalton Trans. 44 (2015) 2122–2131.
[20] F. Franco, M.F. Pinto, B. Royo, J. Lloret-Fillol, Angew. Chem. Int. Ed. 57 (2018) 4603–4606.
[21] H.A. Petersen, T.H.T. Myren, O.R. Luca, Inorganics 8 (2020) 62.
[22] T.H.T. Myren, A.M. Lilio, C.G. Huntzinger, et al., Organometallics 38 (2018) 1248–1253.
[23] J.A. Therrien, M.O. Wolf, Inorg. Chem. 56 (2017) 1161–1172.
[24] H.H. Huang, M. Dai, L. Liu, et al., Catal. Sci. Technol. 11 (2021) 874–885.
[25] X.B. Lan, Z. Ye, J. Liu, et al., ChemSusChem 13 (2020) 2557–2563.
[26] F. Franco, M.F. Pinto, B. Royo, J. Lloret-Fillol, Angew. Chem. Int. Ed. 57 (2018) 4603–4606.
[27] C. Costentin, S. Drouet, M. Robert, J.M. Saveant, J. Am. Chem. Soc. 134 (2012) 11235–11242.
[28] E.S. Rountree, B.D. McCarthy, T.T. Eisenhart, J.L. Dempsey, Inorg. Chem. 53 (2014) 9983–10002.
[29] C. Costentin, J.M. Savéant, ChemElectroChem 1 (2014) 1226–1236.
[30] K.S. Rawat, A. Mahata, I. Choudhuri, B. Pathak, J. Phys. Chem. C 120 (2016) 8821–8831.
[31] G.K. Rao, W. Pell, I. Korobkov, D. Richeson, Chem. Comm. 52 (2016) 8010–8013.
[32] M.L. Clark, P.L. Cheung, M. Lessio, et al., ACS Catal. 8 (2018) 2021–2029.
[33] H.Y. Kuo, S.E. Tignor, T.S. Lee, et al., Dalton Trans. 49 (2020) 891–900.
[34] T.H.T. Myren, A. Alherz, J.R. Thurston, et al., ACS Catal. 10 (2020) 1961–1968.
[35] T. Lu, F. Chen, J. Theor. Comput. Chem. 11 (2012) 163–183.
[36] T. Lu, F. Chen, Acta Phsy. Chim. Sin. 28 (2012) 1–18.
[37] T. Lu, F. Chen, J. Comput. Chem. 33 (2012) 580–592.
[38] W. Luo, M. Sankar, A.M. Beale, et al., Nat. Commun. 6 (2015) 6540.